A low dimensional model for shear turbulence in Plane Poiseuille Flow: an example to understand the edge

Fellow: Giulio Mariotti, Advisor: Norman Lebovitz

September 30, 2011

1 Introduction

Recent studies of turbulent transition in shear flows [12, 10] have highlighted the presence of a peculiar feature in the phase space: the edge of chaos. The edge of chaos, or simply the edge, is a codimension one invariant set embedded in the basin of attraction of the laminar state, which divides this basin in two subregions: one where orbits decay directly and quite rapidly, and a second where they decay indirectly and more slowly. In terms more familiar to fluid mechanics, the edge divides initial flow conditions that relaminarize rapidly from initial flow conditions that experience transient turbulence and eventually relaminarize.

The edge behavior has been identified both in Direct Numerical Simulations (DNS) [10, 11, 9] and in low dimensional models [12]. In both cases the edge coincides with the stable manifold of an invariant object, the edge state [12], which can be either a simple fixed point [11], a periodic orbit or a higher-dimensional chaotic invariant set [12, 10].

Even though DNS constitutes the ultimate tool to explore turbulence, low dimensional models offer precious insights and analogies on the nature of the edge. A seminal contribution is Waleffe's model for Couette flow [14] (W97), based on a Galerkin's truncation of the NS equations. The modes chosen for the truncation stem from a self sustained process between streamwise rolls, streamwise streaks, and streaks instabilities, a triad considered fundamental in turbulent transition [3]. Waleffe proposed an eight modes model and a further reduction to a four modes model, both of which showed a lower branch family of saddle points and an upper branch family of stable or unstable fixed points, analogous to the upper and lower branches of traveling waves found in DNS [15, 16]. The presence of a dual relaminarization behavior in the W97 model, 'direct' and through 'transient-turbulence', was identified in [1], while the edge structure was studied recently in [4]. A dual relaminarization behavior was also found in a nine modes variation of W97 [6, 7].

A question about the edge remains open: if the edge divides the phase space in two regions, how do trajectories that experience transient turbulence relaminarize? It was initially proposed [12] that initial conditions that experience transient turbulence lie close to the edge, specifically between two symmetric parts of it, but in the laminar basin. The longer relaminarization time was explained by the fractal structure of the edge. It has been suggested [10] that 'the stable manifold of the laminar profile and the stable manifold of the edge state have to intermingle tightly in the region with turbulent dynamics'.

A dynamical description of the edge's 'intermingling' has been drawn by a simple two dimensional model [5], which features only linear and quadratic terms, non-normal matrix for the linear terms and energy conserving nonlinear terms. The idea is that the edge, i.e. the stable manifold of the edge state, does not extend indefinitely over the whole phase space. Indeed, the model shows that part of the stable manifold of a lower branch fixed point, i.e. the edge, coincides with the unstable manifold of an upper branch fixed point. The basic mechanism of the edge is hence the following: trajectories starting below the stable manifold approach the origin directly, while trajectory starting above the stable manifold have to travel around the upper branch fixed point in order to reach the origin. To complicate further the situation, the stable manifold can spiral around the upper branch fixed point. As a result, orbit starting between the folds of the stable manifold will experience a longer path to the origin, enhancing the edge behavior.

Here we study a six order truncated model of Plane Poiseuille Flow with free-slip boundary conditions. The basic structure is analogous to W97 and indeed the models shows analogous dynamical characteristics. In addition, the model has striking similarities with the two dimensional model in [5]. The main purpose of this work is to identify the edge-like behavior and to explain it in terms of basic dynamical systems objects. This description will hopefully facilitate the understanding the edge behavior in more complex systems, such as the full NS equations.

2 Model description

The coordinates' system is chosen such that x in the streamwise direction, y in the wall-normal direction, and z in the spanwise direction. The domain is $x \in [0, L_x]$, $y \in [-1, 1]$, and $z \in [0, L_z]$, where $L_x = \frac{2\pi}{\alpha}$, $L_z = \frac{2\pi}{\gamma}$. The vertical wave number, β, is chosen equal to $\pi/2$, while the x and z wavenumbers are initially left unconstrained. Periodic boundary conditions are imposed along x and along z. Six solenoidal modes are introduced:

$$\phi_1 = \begin{bmatrix} \sqrt{2}cos(\beta y) \\ 0 \\ 0 \end{bmatrix}, \tag{1}$$

$$\phi_2 = \begin{bmatrix} 2\sqrt{2}cos(\gamma z)sin(2\beta y)sin(\beta y) \\ 0 \\ 0 \end{bmatrix}, \tag{2}$$

$$\phi_3 = \frac{2}{c_3} \begin{bmatrix} 0 \\ \gamma sin(2\beta y)cos(\gamma z) \\ -2\beta cos(2\beta y)sin(\gamma z) \end{bmatrix}, \tag{3}$$

$$\phi_4 = \begin{bmatrix} 0 \\ 0 \\ 2cos(\alpha x)sin(2\beta y) \end{bmatrix}, \tag{4}$$

$$\phi_5 = \frac{\sqrt{2}}{c_5} \begin{bmatrix} 2\gamma cos(\alpha x)sin(\gamma z)sin(\beta y) \\ 0 \\ -2\alpha sin(\alpha x)cos(\gamma z)sin(\beta y) \end{bmatrix}, \tag{5}$$

$$\phi_6 = \frac{2\sqrt{2}}{c_6}\begin{bmatrix} -\alpha\beta cos(\alpha x)sin(\beta y)sin(2\gamma z) \\ (\alpha^2+\gamma^2)sin(\alpha x)cos(\beta y)sin(2\gamma z) \\ \beta\gamma sin(\alpha x)sin(\beta y)sin(\gamma z)^2 \end{bmatrix}, \tag{6}$$

with the following normalization coefficients:

$$c_3^2 = 4\beta^2+\gamma^2, c_5^2 = \gamma^2+\alpha^2, c_6^2 = \alpha^2\beta^2+\gamma^4+2\gamma^2\alpha^2+\alpha^4+3/4\beta^2\gamma^2. \tag{7}$$

The first three modes are intended to represent respectively the mean streamwise flow, the streamwise streaks, and the streamwise rolls. The last three modes are intended to represent the 1D, 2D and 3D streak instabilities. The mean flow is approximated by a cosine. The maximum difference in the streamwise velocity is found between the walls, $y = 1$ and the center line, $y = 0$. As a consequence, the roll capable of the most mixing has a wavelength equal to $\beta/2$ (Fig. 1). As a comparison, the most mixing efficient roll in Couette Flow has wavelength equal to β. The resulting Galerkin representative of the streaks, ϕ_2, has a maximum at $y = \pm\frac{2}{\pi}\arccos\left(\frac{1}{\sqrt{3}}\right) \sim \pm 0.61$, which is closer to the wall than the centers of the rolls, $y = \pm\frac{1}{2}$ (Fig. 1).

The roll mode ϕ_3 has free-slip boundary condition in the z direction, and the 2D and 3D streaks instability modes, ϕ_5 and ϕ_6, have free-slip boundary conditions in both the x and z direction. The six modes are drawn from the 'shift-reflect' class, i.e., equivalent under the transformation:

$$[u(x,y,z); v(x,y,z); w(x,y,z)] \rightarrow [u(x+L_x/2, y, -z); v(x+L_x/2, y, -z); -w(x+L_x/2, y, -z)], \tag{8}$$

where u, v, and w are the velocity components along x, y, and z.

Assuming that the modes are fully capturing the dynamics of interest, the velocity field is truncated to the following finite summation:

$$\mathbf{u}(\mathbf{x}, t) = \sum_{i=1}^{N} X_i(t)\phi_i(\mathbf{x}), \tag{9}$$

where X_i is the amplitude of the mode ϕ_i and N is the number of modes, here equal to 6. The truncated velocity is then substituted in the Navier Stokes equations,

$$\frac{\partial \mathbf{u}}{\partial t} + \mathbf{u}\cdot\nabla\mathbf{u} = -\nabla p + \frac{1}{R}\nabla^2\mathbf{u} \quad + F(y)\hat{\mathbf{X}}, \tag{10}$$

and the resulting equation (10) is projected into the each mode ϕ_k, by setting the inner product of (10) and ϕ_k equal to zero. The spatial integration of the inner product removes the space-dependence and the procedure yields a system of N coupled ODEs for the amplitude X_i. The partial time derivative in (10) becomes the total time derivate in the ODEs, the laplacian becomes a linear term, while the advection becomes non-linear terms. Because of the solenoidal condition of the modes and the boundary conditions, the pressure term does not appear in the ODEs, while the body force becomes an inhomogeneous term.

Utilizing the modes 1-6, we obtain the following system of ODEs for the amplitudes X_i,

$$\dot{\mathbf{X}} = A\mathbf{X} + g(\mathbf{X}) + \frac{k_1}{R}\hat{X}_1. \tag{11}$$

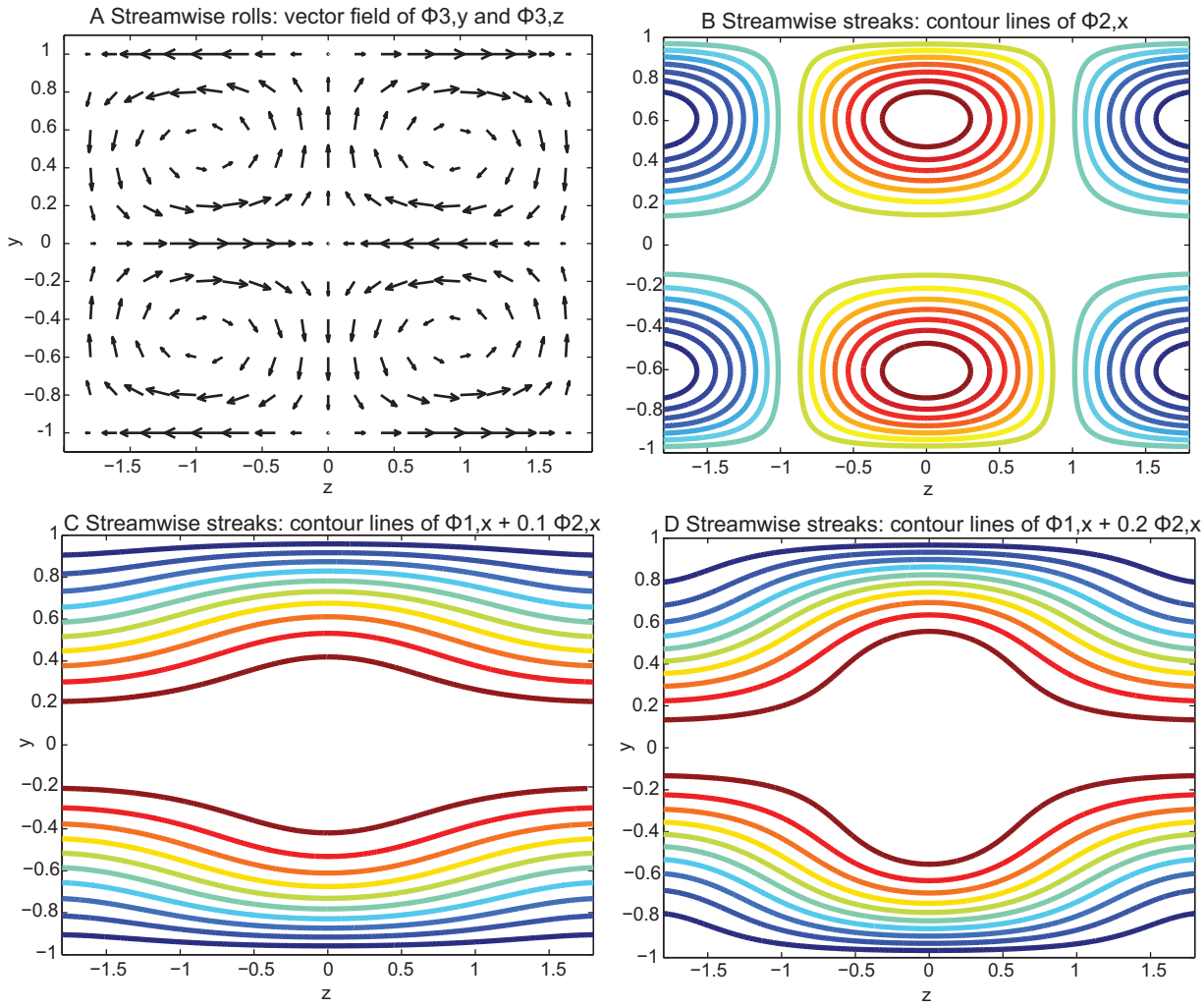

Figure 1: A) Vector field of the streamwise rolls (y and z component of ϕ_3). B) Contour lines of the streamwise streaks (x component of ϕ_2). C,D) Redistribution of the streamwise velocity under the combination of the mean flow and the stramwise streaks, for $X_2 = 0.1$ and $X_2 = 0.2$, with $X_1 = 1$. Contour lines every 0.1, from 0 at $y = \pm 1$ to 1 at $y = 0$.

The forcing term is present only in the direction of the mean flow mode. The matrix A describes the viscous dissipation,

$$A_{i,j} = -\delta_{i,j}\frac{k_i}{R}, \tag{12}$$

where,

$$\boldsymbol{k} = \begin{bmatrix} \beta^2 \\ 5\beta^2+\gamma^2 \\ c_3^2 \\ \alpha^2+4\beta^2 \\ \alpha^2+\beta^2+\gamma^2 \\ (\alpha^2+\beta^2)+(\gamma^2(4c_5^4+\beta^2(4\alpha^2+\gamma^2)))/c_6^2 \end{bmatrix}.$$

The operator g includes the non-linear terms,

$$g(\mathbf{X}) = \begin{bmatrix} -\sigma_0 X_2 X_3 \\ \sigma_0 X_1 X_3 - \sigma_1 X_4 X_5 \\ -(\sigma_4+\sigma_5) X_5 X_6 \\ \sigma_2 X_2 X_5 - \sigma_3 X_1 X_6 \\ (\sigma_1-\sigma_2) X_2 X_4 + (\sigma_4-\sigma_6) X_3 X_6 \\ (\sigma_5+\sigma_6) X_3 X_5 + \sigma_3 X_1 X_4 \end{bmatrix},$$

with the following coefficients:

$$\sigma_0 = \frac{\beta\gamma}{c_3}, \sigma_1 = \frac{\gamma^2}{c_5}, \sigma 2 = \frac{\alpha^2}{c_5}, \sigma_3 = \frac{\gamma\alpha\beta}{2c_6}, \sigma_4 = \frac{\beta^2(4\alpha^2+5\gamma^2)\alpha}{2c_3c_5c_6}, \sigma_5 = \frac{(\beta^2-\alpha^2-\gamma^2)\gamma^2\alpha}{2c_3c_5c_6}, \sigma_6 = \frac{\gamma^2\beta^2\alpha}{4c_3c_5c_6}. \tag{15}$$

The non-linear terms are quadratic and conserve energy, i.e. $\langle \mathbf{X} \cdot g(\mathbf{X}) \rangle = 0$. The system of ODEs shows three symmetries: S_1=diag(1,1,1,-1,-1,-1), S_2=diag(1,-1,-1,1,-1,1), and S_3=diag(1,-1,-1,-1,1,-1). The last symmetry comes from the product of the first two. These symmetries are undoubtedly inherited from the shift-reflect symmetry, but the derivation has not been done.

Finally, the transformation $X_1 \to X_1 + 1$ is introduced, so that the laminar state corresponds to $\mathbf{X} = 0$.

3 Analysis of the system

The matrix of the system linearized around the laminar state is non-normal, because of the component $\sigma_0 X_1 X_3$ in the second ODE of (11). The laminar state is a fixed point, linearly stable for all R. It is evident that the model is not able to reproduce the linear instability of the laminar state found in Plane Poiseuille Flow for $R > 5772$ [8]. However, it is widely accepted that this instability is not significant for transition to turbulence.

The analytical solution for the steady state of the system (11) is found to be a polynomial of 8^{th} order in X_5. Under the explored range of value for the parameter α, γ and R, no real solutions are found, implying that the system (11) has no fixed points other than the laminar point. Also an asymptotic analysis shows no presence of fixed points. In order

to reduce the number of free parameters, the wavelengths are set constant, $\gamma = 5/3$ and $\alpha = 1.1$, corresponding to the values used for the Couette flow in W97 [14].

The search of other non-trivial solutions is initially performed sampling the direction of the maximum transient linear growth. An approximation of this direction is found to be $\hat{X_3}$, i.e. the rolls component. However, perturbing the laminar state in only one direction is not sufficient to find non-laminar solutions. In fact, the modes $X_{1,2,3}$ constitute a closed set when the initial value of the modes $X_{4,5,6}$ is zero. We therefore introduce a small perturbation, $O(10^{-3})$, on the modes $X_{2,4,5,6}$, and a greater perturbation, $O(10^{-1})$, on the X_3 mode. Fixing $R = 500$, a stable periodic orbit is found.

4 Bifurcation analysis

The bifurcations of the stable orbit were followed using the continuation software MatCont [2], using R as control parameter. A saddle node bifurcation appears for $R > R_{sn} \sim 291.7$, giving birth to two branches of periodic orbits (Fig. 2A). The lower branch (PO_{lb}), closer to the laminar state, is unstable for all R, with only one real Floquet multiplier greater than one (Fig. 2C). The upper branch (PO_{ub}) is initially unstable, with two real multipliers greater than one (Fig. 2D). The two multipliers readily become complex conjugate for $R > R_c \sim 292.4$, but they remain greater than one. At $R > R_t \sim 305.5$ the two complex conjugate multipliers become smaller than one, and the periodic orbit becomes stable. Because of the system symmetries, two other couples of upper and lower branches periodic orbits are present.

The bifurcation portrait shows some similarities with the model W97, in which a saddle-node bifurcation gives birth to two branches of fixed points. Also for the W97 model, the lower branch is always unstable, with only one unstable direction, and the upper branch is initially unstable, with two unstable directions. The upper branch is initially an unstable node, and turns readily into an unstable spiral, when the two positive eigenvalues become complex conjugate. For higher value of R the spiral node becomes stable through a Hopf bifurcation. The analogy between the two models is clear when fixed points are replaced with periodic orbits.

4.1 Bifurcation at R_t

When R exceeds R_t, a bifurcation takes place: the laminar state ceases to be the only attracting state and PO_{ub} introduces an additional basin of attraction. A slice of the two basins in the $X_1 - R$ plane, with components $X_{2,3,4,5,6}$ kept fixed, is plotted in Figure 3. The boundary is identifiable using the time needed for the orbit to come arbitrarily close to the origin (relaminarization time). Trajectories starting inside the basin of attraction of PO_{ub} have a relaminarization time equal to infinity or to the maximum simulation time. The identification of the basin boundary is complicated, as usual, by the long transient time of trajectories starting close to the basin boundary. As expected the new basin of attraction appears around $R = R_t$, and expands for increasing value of R.

Are there structures embedded in the boundary of the basin of attraction? Since the bifurcation at $R = R_t$ is a subcritical Neimark-Sacker type, we expect the appearance of an invariant two-dimensional torus for $R > R_t$. Indeed we found a periodic orbit lying on

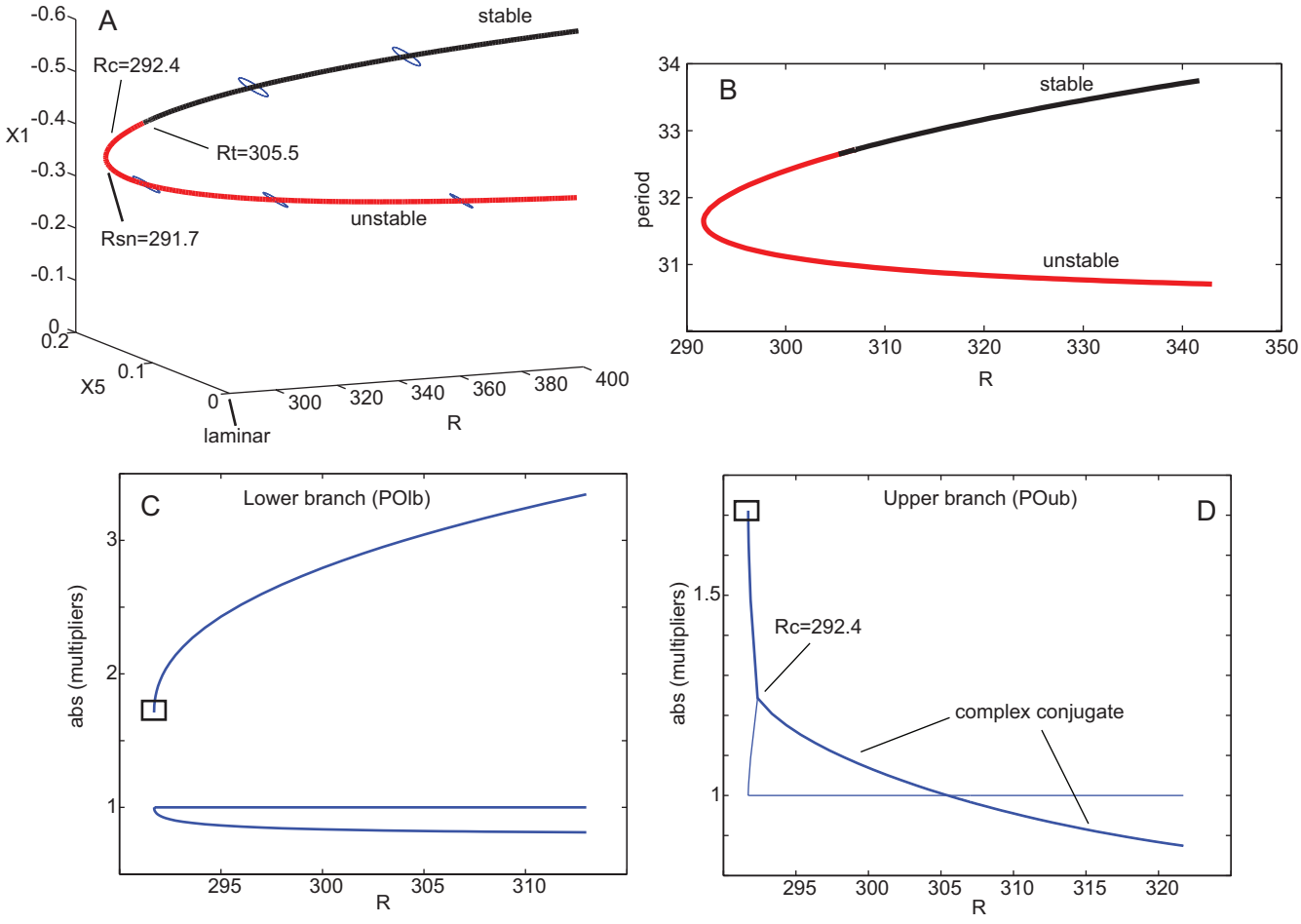

Figure 2: A) Coordinate X_1 and X_5 of the center of the upper and lower branches periodic orbits for different value of R. The blue circles represent the periodic orbits at selected value of R. The coordinate $X_{2,3,4,6}$ of the center of both periodic orbits is identically zero for all R. B) Period of the upper and lower branch periodic orbits. C,D) First three greater multipliers of the upper and lower branch periodic orbits. The values in the squares are the same, i.e. the multipliers coincide at the saddle node bifurcation.

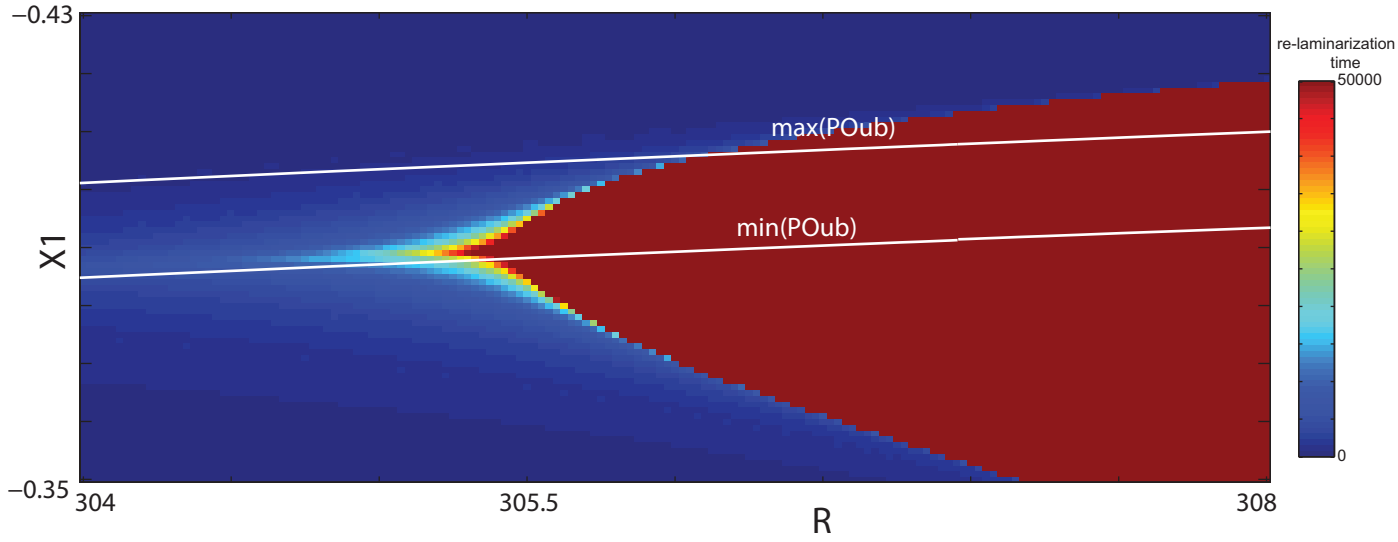

Figure 3: Each grid square is colored to show the lifetime before relaminarization for trajectory with initial conditions X_1 and parameter R. The other initial conditions are constant for each cells, $X_2 = -0.0511$, $X_3 = -0.0391$, $X_4 = 0.0016$, $X_5 = 0.1924$, $X_6 = 0.1260$, which correspond to a point on PO_{ub}. The other parameters are $\gamma = 5/3$, and $\alpha = 1.1$. A section of the basin of attraction of PO_{ub} coincides approximately with red region. The lines represent the projection of the minimum and maximum value of PO_{ub}.

a torus embedded in the basin boundary. This orbit was found bisecting initial conditions on different sides of the basin boundary. The orbit on the torus for $R = 307.0$ is shown in Figure 4D. The torus orbit has a high-frequency modulation with a period approximately equal to that of PO_{ub}. The total period of the torus orbit is approximately then times this high-frequency modulation. The multipliers of the orbit are $1.19 \pm 0.45i$; 1; $2\ 10^{-5}$; 1 10^{-10}; $5\ 10^{-8}$. The torus is therefore unstable, with a very attracting stable manifold.

Unfortunately, we were not able to continuate the torus orbit for different value of R using Matcont. Computing the torus orbit with the bisection technique for different value of R, we found that the torus shrinks for decreasing values of R and collapses to PO_{ub} at $R = R_t$. We also found that the period of the orbit on the torus can change discontinuously with R. A complete investigation of the torus is left to other studies.

4.2 Description of the periodic orbit

For completeness, a brief description of the periodic orbits is presented. The period at the saddle node bifurcation is ∼31.8 time units. The period of PO_{ub}, T, increases monotonically with R, while the period of PO_{lb} decreases monotonically with R (Fig. 2B), both approaching an asymptotic value. The structure of PO_{ub} and PO_{lb} is similar for all values of R (Fig. 4). The center of both PO_{ub} and PO_{lb} has components $X_{2,3,4,6}$ equal to zero and components $X_{1,5}$ different from zero. In addition, the period of the components X_1 and X_5 is half the period of the other 4 components, i.e. the period of of X_1 and X_5 alone is half the period of the full orbit. The different behavior of the mode X_1 and X_5 compared to the

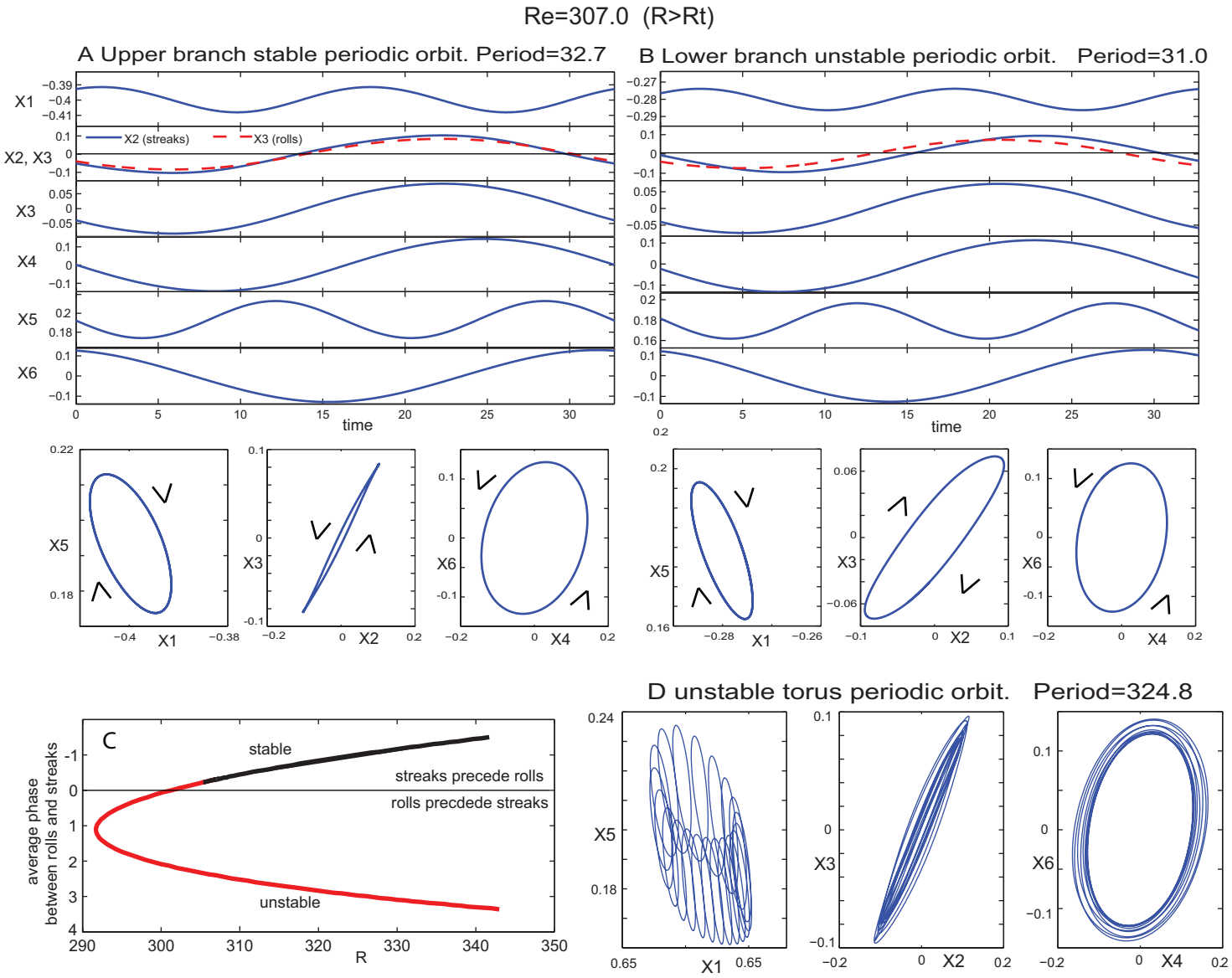

Figure 4: A) Upper branch stable periodic orbit, $R = 307.0$ ($R > R_t$). The orbit in the $X_2 - X_3$ plane is counter clockwise. B) Lower branch unstable periodic orbit. The orbit in the $X_2 - X_3$ is clockwise. C) Average phase lag between the mode X_2 (streaks) and mode X_3 (rolls). Positive lag means that the rolls precede the streaks. D) Periodic orbit on the torus, embedded in the basin boundary of PO_{ub}.

other modes emerges from the symmetry S_3. We have in fact that $S_3(\mathbf{X}(t)) = \mathbf{X}(t + T/2)$, i.e. $S_3(\mathbf{X}(t))$ is not a different periodic solution but just the original solution translated by half period. This implies that the mean of $X_{2,3,4,6}$ over a period must vanish. In general, we don't expect this to be a common feature in other low dimensional models.

A particular behavior of the streaks and rolls mode, ϕ_2 and ϕ_3, was noticed: they seem to have a different relative phase in the stable and unstable periodic orbit. As shown in Figure 4A and B, the streaks precede the rolls in the stable orbit, while the rolls precede the streaks in the unstable orbit. In the $X_2 - X_3$ plane, the former situation corresponds to a counter clockwise rotation of the trajectory and the latter to a clockwise rotation. The phase lag of the streaks relative to the roll is quantified with the maximum of the cross-correlation between X_2 and X_3:

$$\varphi = max(t) \int_T X_3(\tau) X_2(\tau + t) d\tau, \tag{16}$$

The lag of the streaks is positive for the whole lower branch and for most of the unstable part of the upper branch. For R just before R_t the lag of the streaks turns negative, and remains negative for the remaining part of the upper branch. The physical interpretation of these behaviors is not clear, and will not be considered further in this work.

5 Structure of the edge

The rest of this work is devoted to the search edge-like structures in the phase space.

5.1 $R > R_t$

We first consider the case of $R > R_t$, when both a stable and an unstable periodic orbit are present. The lifetime before relaminarization is used to map the phase space (see [6, 12, 10, 13]). The coordinates X_1 and X_5 seem an intuitive choice, given their different behavior with respect to $X_{2,3,4,6}$. Figure 5 shows the relaminarization time for different fixed values of $X_{2,3,4,6}$, keeping R fixed, equal to 307.0. Two regions are distinguished: D, where orbits are attracted to the stable periodic orbit PO_{ub}, and B, where orbits are attracted to the origin in a finite time. In addition, two subregions can be distinguished in B: B_s, where orbits tend to the origin in a relatively short time, and B_l, where orbits tend to the origin in a longer time. In general, while trajectories starting in B_s proceed almost directly to the origin, trajectories starting in B_l take a more convoluted path to the origin, causing the longer relaminarization time.

The different time and pattern of relaminarization in B is now analyzed. Starting with a trajectory in B_s (e.g. trajectory p_1 in Fig. 6A), we move the initial condition toward the basin D. We intersect a point after which orbits take a considerable longer path before approaching the laminar state. Using a bisection technique [12], we identify a point in the phase space of initial conditions, say x_0, which determines a sudden change: a trajectory starting just below x_0, x^-, approaches the origin quite directly, while a trajectory starting just above x_0, x^-, takes a longer path to the origin (Fig. 6B).

Both trajectory x^- and x^+ approach PO_{lb} arbitrarily close. Before the two trajectories collapse into PO_{lb}, they separate: x^- goes directly to the origin while x^+ swings up, visits

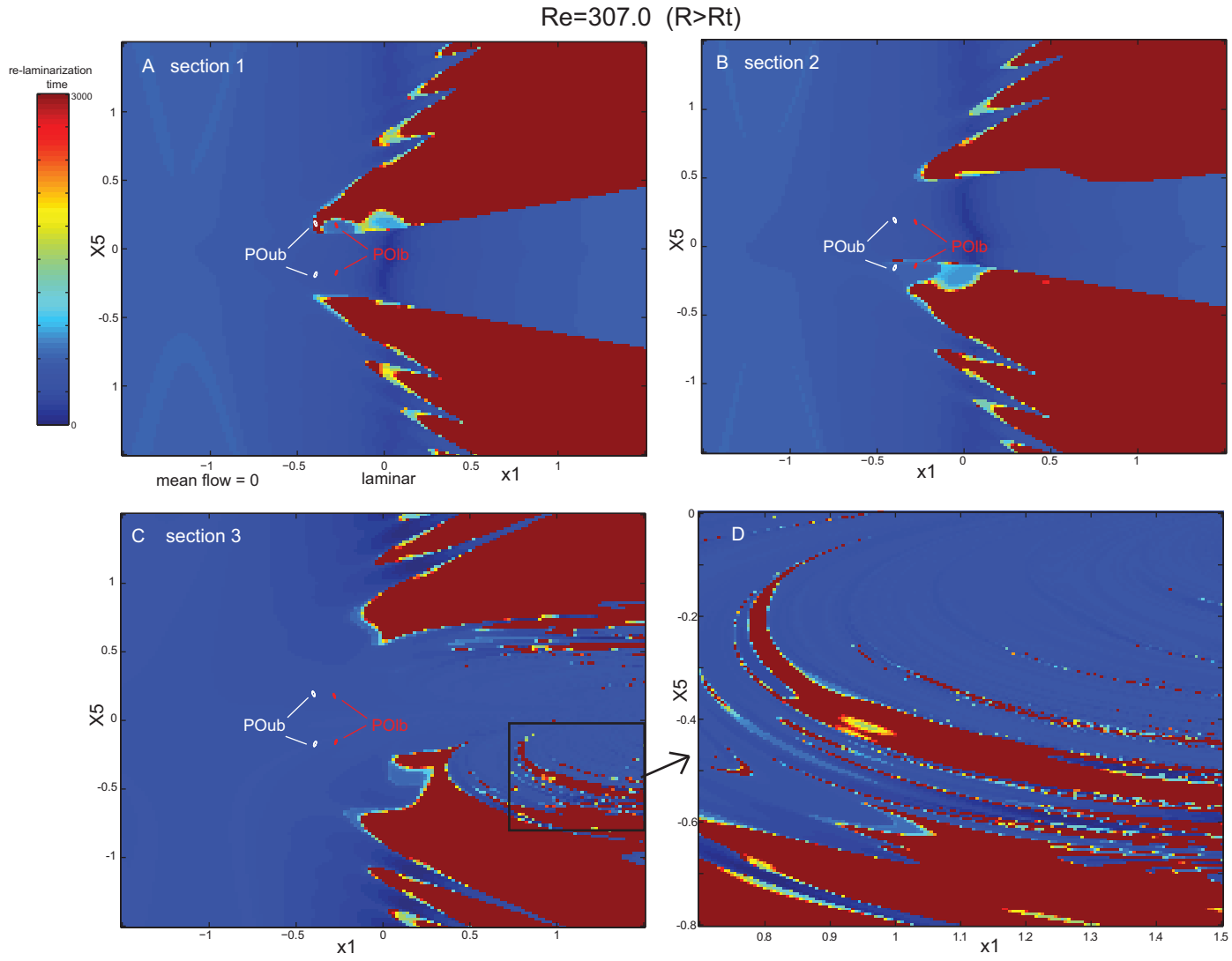

Figure 5: A) Two dimensional sample of the phase space, with the laminar state at the origin, for $R = 307.0$ ($R > R_t$). Each grid square is colored to show the lifetime before relaminarization for trajectory with initial conditions X_1 and X_5 and the center of the cell. The other initial conditions are constant for each cells: $X_2 = -0.0511$, $X_3 = -0.0391$, $X_4 = 0.0016$, $X_6 = 0.1260$, which correspond to a point on PO_{ub}. The other parameters are $\gamma = 5/3$, and $\alpha = 1.1$. The upper and lower branch periodic orbits are projected into this plane. B,C) Same as in A, with the coordinate X_3 increased by 0.1 and 0.5 respectively. D) Detail of C.

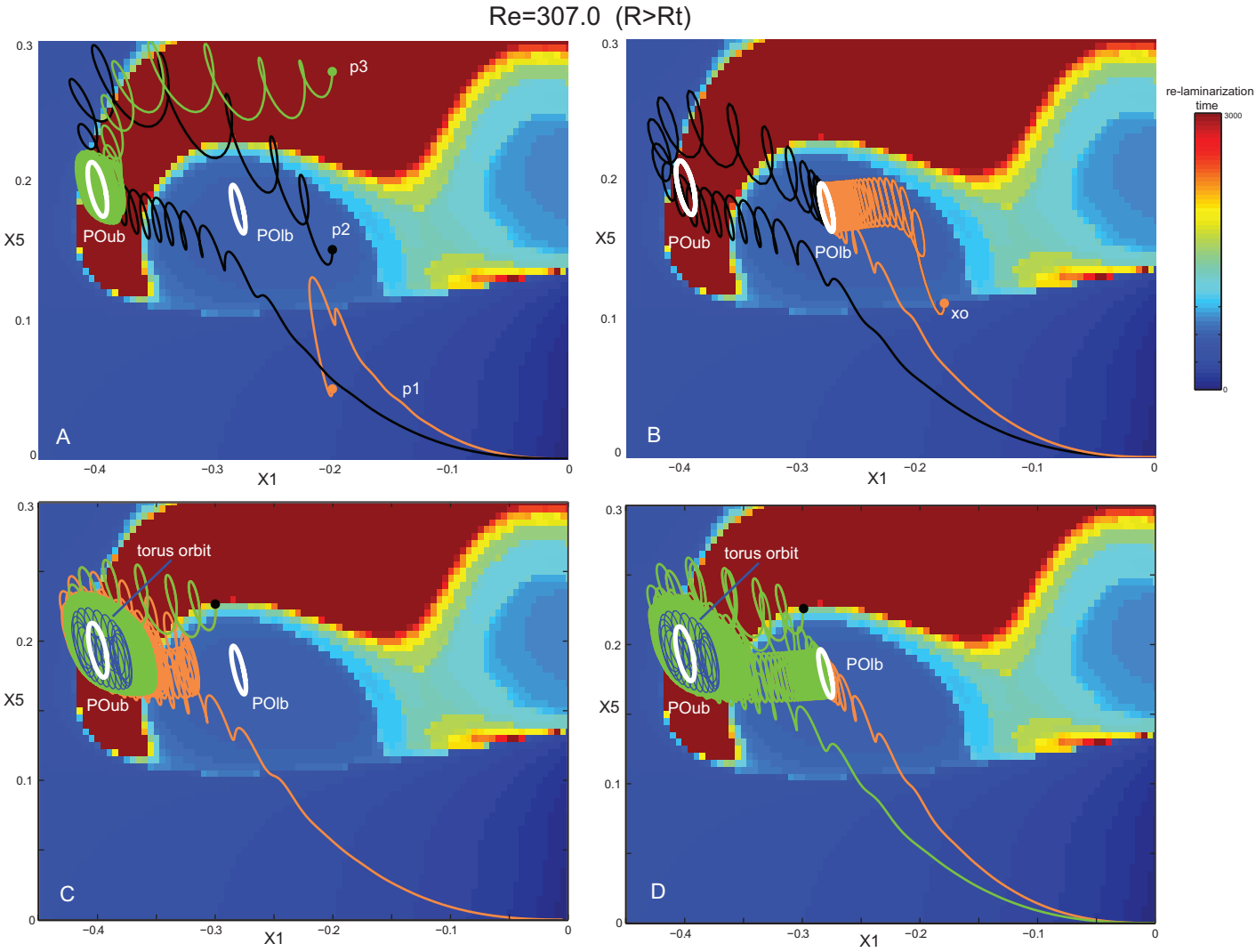

Figure 6: On the background, lifetime of trajectories before relaminarization, for $R = 307.0$, as in Figure 5. The upper and lower branch periodic orbits, the torus orbit and some significant trajectories are projected into this plane. A) Trajectory p_1 relaminarizes following a short path; trajectory p_2 relaminarizes following a longer path, visiting the region near PO_{ub} and the torus orbit; trajectory p_3 converges to PO_{ub}. B) Trajectories starting infinitesimally close to each other first approach PO_{lb} and then diverge into different path toward the origin. C,D) Trajectories near the basin boundary of PO_{ub} have convoluted paths around PO_{ub} and the torus orbit, and some of them approach PO_{lb} before relaminarization.

the region near the torus orbit and eventually converges to the origin. The fact that both x^- and x^+ initially converge to PO_{lb} implies that the point x_0 lies on the stable manifold of PO_{lb}, $SM(PO_{lb})$. The different trajectory behavior after PO_{lb} is evidently dictated by the presence of two branches of the unstable manifold of PO_{lb}, $UM(PO_{lb})$.

Because both x^- and x^+ belong to the laminar basin, the point x_0 has the nature of an edge: trajectories starting infinitesimally close but on two opposite sides of x_0 have different finite-time, but same asymptotic dynamics. This result agrees with the finding that the edge coincides with the stable manifold of an invariant object [10, 9, 6, 12], which in this case corresponds to a lower branch of unstable periodic orbits. In addition, the fact that the trajectory x^+ is approaching the region of PO_{ub} suggests the presence of a connection between the upper and lower periodic orbits.

5.1.1 The way toward multiple edges

In order to navigate the variety of relaminarization patterns in B, we analyze two transects of initial conditions crossing ∂D. For simplicity, the two transects are chosen in the X_1 and X_5 direction, with all the other initial conditions kept fixed (Fig. 7). The first point on the transects, p_i, corresponds to a trajectory that relaminarizes 'directly', while the last point on the transects, p_e, corresponds to a trajectory that converges to PO_{ub}. Trajectories are described using two parameters: the time to relaminarization, and the maximum value achieved by the coordinate X_5, a footprint of the trajectory history.

The outcomes for both transects are similar. The relaminarization time is minimum for p_i and maximum, equal to the simulation time, for p_e. The lifetime of the initial conditions between p_i and p_e is characterized by 'steps' and 'spikes'. Starting from p_i and moving toward p_e, the lifetime is approximately constant, it suddenly increases and shortly after decreases. The lifetime then remains steady, higher than before the peak, approximately constant until the next peak. Increasing the number of bisection points, we found that points starting close to each peak come arbitrarily close to PO_{lb}. The interpretation is straightforward: at every peak the vector of initial conditions is intersecting a different fold of $SM(PO_{ub})$. Points lying just below or above $SM(PO_{ub})$ are attracted to PO_{ub} and then are captured by the two opposite arcs $UM(PO_{ub})$. The peak of $max(X_5)$ is evidently a trajectory captured by the arc of $UM(PO_{ub})$ leaving in the direction opposite to the origin.

What happens between the different folds of $SM(PO_{lb})$? We noticed that after every peak in the relaminarization time, the orbit make an 'extra loop' around the torus orbit. The consequence of these extra loops is manifested as the 'steps' in relaminarization time. Therefore every fold of $SM(PO_{lb})$ determines a band of increasing relaminarization time. This suggests that $SM(PO_{lb})$ is wrapped around ∂D. Different folds of $SM(PO_{lb})$ appears also when other coordinates are chosen to section the phase space (Fig. 8). For example, the first 4 folds of $SM(PO_{lb})$ are plotted in Figure 8D.

It comes natural to ask what relationship is present between $SM(PO_{lb})$ and the orbits on the basin boundary of PO_{ub}. A simple interpretation would be that $SM(PO_{lb})$ coincides with the unstable manifold of the orbit on the torus, $UM(T)$. The spacing between the folds supports this idea. We found that the distance between the folds is in a geometric succession, approximately equal for both transects studied. Indeed the folds of an unstable manifold spiraling out of a periodic orbit are expected to be in a geometric succession.

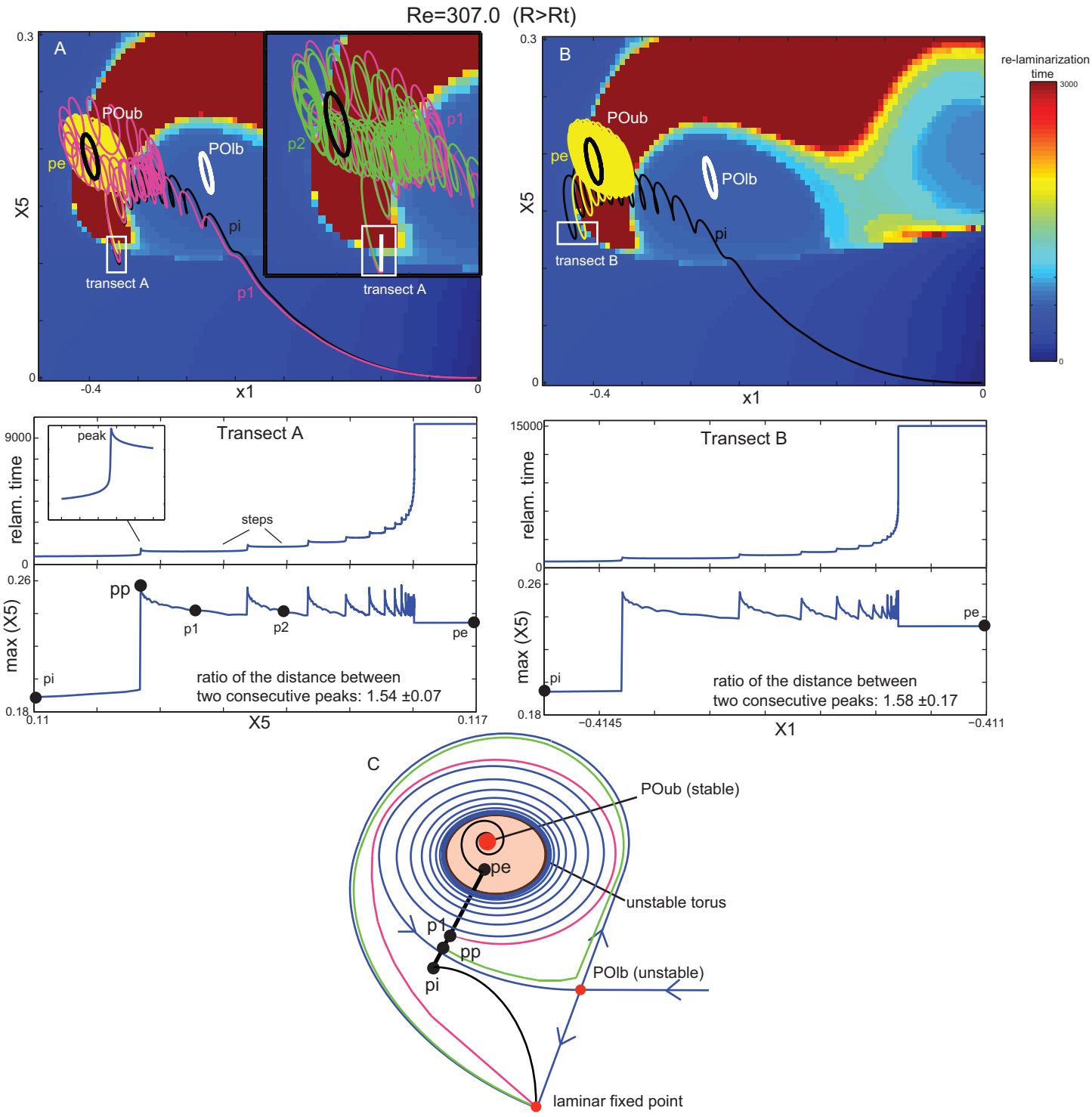

Figure 7: A,B) Lifetime of trajectories, as in Figure 5. Some trajectories and the periodic orbits are projected into the plane. Two transects of initial conditions crossing ∂D are analyzed. Transect A is aligned along the direction X_5; transect B is aligned along the direction X_1. All the other initial conditions are kept fixed. The first point on both transects, p_i, corresponds to a trajectory that relaminarizes 'directly', while the last point, p_e, corresponds to a trajectory that converges to PO_{ub}. Trajectories corresponding to the initial conditions on the transects are described using two parameters: the time to relaminarization, and the maximum value achieved by the coordinate X_5, a footprint of the trajectory history. C) Cartoon of the phase space, with the laminar fixed point, PO_{ub}, PO_{lb}, the torus orbits and some trajectories as an example.

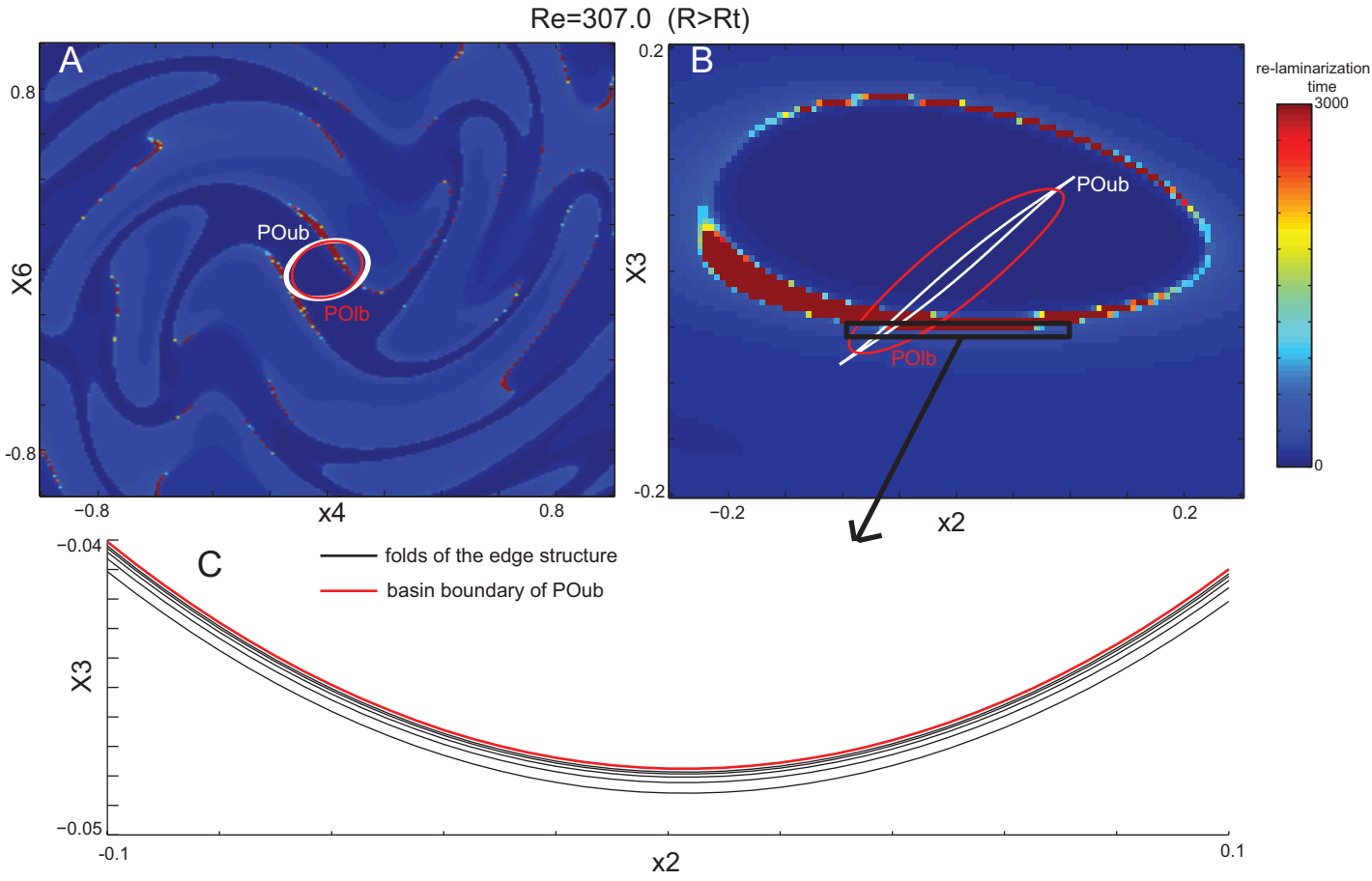

Figure 8: A,B) Lifetime of trajectories and projection of PO_{ub} and PO_{lb}, as in Figure 5, but utilizing different coordinates: X_4-X_6, and X_2-X_3. C) Representation of the edge's folds, identified using the 'peaks' of relaminarization time as in Figure 7.

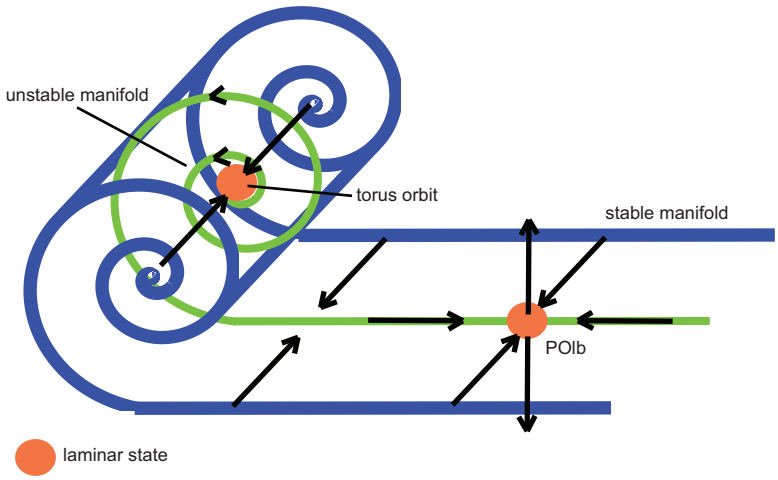

Figure 9: Example of how $UM(PO_{ub})$ can intersect $SM(PO_{lb})$, in a three dimensional case. $UM(PO_{ub})$ lies on a vertical plane and the green line is the intersection.

A cartoon of the various periodic orbits and manifolds is exemplified in Figure 7C. This situation is analogous to the 2D model in [5], where the stable manifold of the lower branch fixed point coincides with the unstable manifold of an unstable periodic orbit.

The situation in our case is more complicated than described above. The edge, which coincides with $SM(PO_{lb})$, has codimension one, i.e. dimension 5 in our system. The torus orbit has two complex conjugate unstable multipliers, at least for the value of R considered. The dimension of $UM(T)$ is 3, considering both the unstable and neutral multipliers. Therefore $UM(T)$ and $SM(PO_{lb})$ cannot coincide. Instead, it is likely that these to objects intersect. A three dimensional cartoon of this intersection is shown in Figure 9.

5.2 $R < R_t$

When R decreases the basin of attraction of PO_{ub} shrinks and eventually disappears for $R < R_t$ (Fig. 3). The origin is a global attractor, except for a measure zero set containing the upper and lower branch unstable periodic orbits. Is the edge structure still present?

5.2.1 $R_c < R < R_t$

First we investigate the case with $R_c < R < R_t$, when the multipliers greater than one are complex conjugate. Again, we use the relaminarization time to map the phase space. All initial conditions relaminarize before the maximum simulation time (Fig. 10), in agreement with the absence of no other basins of attraction besides the laminar one. However, both regions with short, B_s, and long, B_l, relaminarization time persist, indicating the presence of the edge.

We study a transect of initial conditions, with the initial point p_i on B_s and the final point p_e on PO_{ub}. The results are analogous to the case with $R > R_t$: the lifetime of p_i is minimum, the lifetime of p_e is equal to the maximum time allowed by the simulation, and

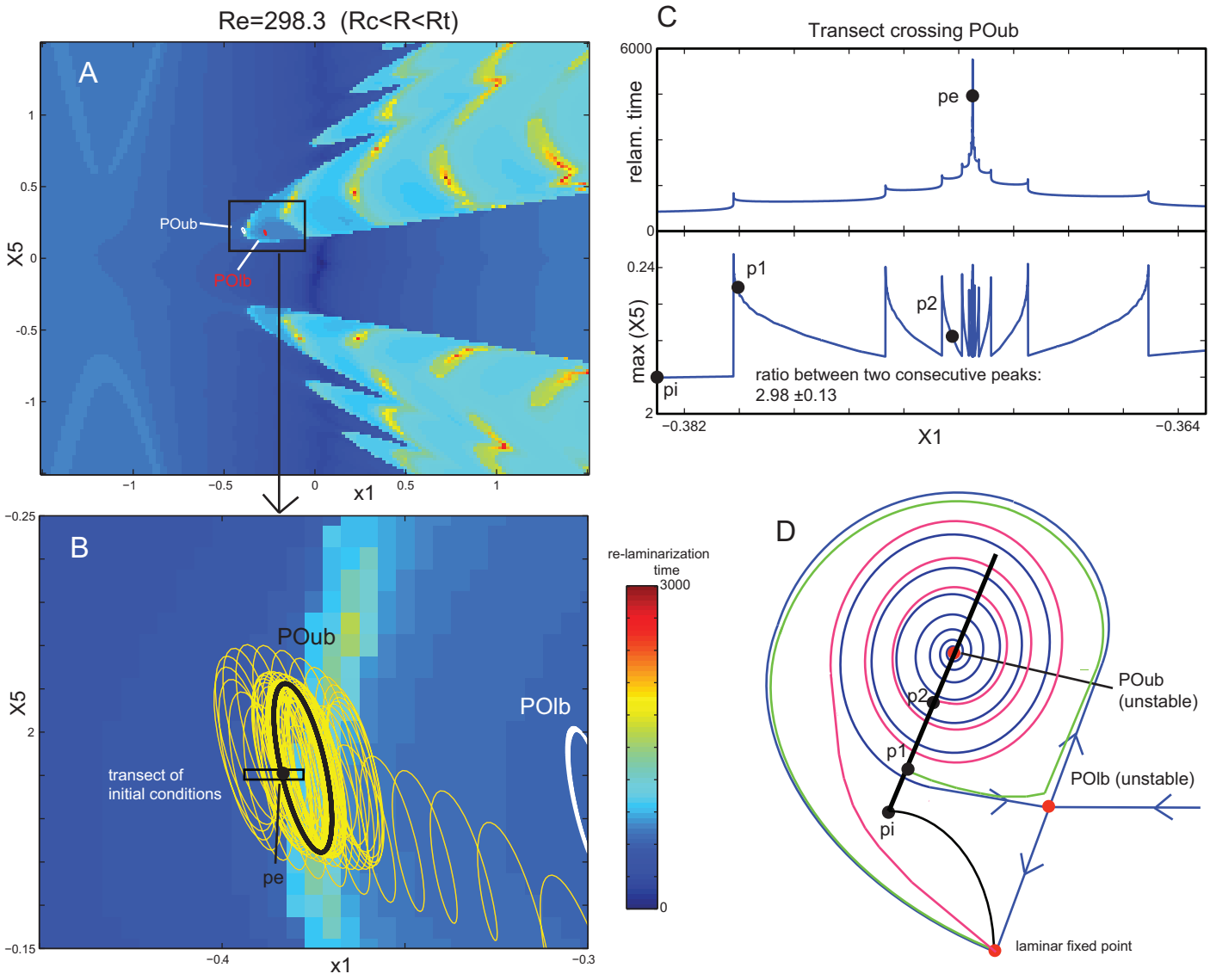

Figure 10: A,B) Lifetime of trajectories and projection of PO_{ub} and PO_{lb}, as in Figure 5, but with $R = 298.3$ ($R_c < R < R_t$). C) Analysis of a transect of initial conditions crossing PO_{ub}. Trajectories corresponding to the initial conditions on the transect are described using two parameters: the relaminarization time and the maximum value achieved by the coordinate X_5. The point p_i corresponds to an initial condition that relaminarize 'directly', while the point p_e corresponds to an initial condition on PO_{ub}. D) Cartoon of the phase space, with the laminar fixed point, PO_{ub}, PO_{lb}. Trajectory p_1 starts close to $SM(PO_{lb})$, trajectory p_2 starts between two folds of $SM(PO_{lb})$.

the lifetime of the initial conditions between p_i and p_e is characterized by 'peaks 'and 'steps'. Also in this case, trajectories associated with the peaks converge toward PO_{lb}, confirming that the transect of initial conditions is intersecting $SM(PO_{lb})$.

The distance between the peaks continues to be in a geometric succession, which suggests that $SM(PO_{lb})$ is spiraling around PO_{ub}. Is $SM(PO_{lb})$ still related to an unstable manifold? Because the torus orbit disappeared, $UM(PO_{ub})$ is the only candidate to consider. Also in this case the dimension of the unstable manifold is 3, less than the dimension of $SM(PO_{lb})$. Again, $UM(PO_{ub})$ cannot coincide with $SM(PO_{lb})$, but it might intersect it. Interestingly, the dimension of $UM(PO_{ub})$ is one unit smaller than the dimension of $SM(PO_{lb})$, and hence $UM(PO_{ub})$ is a potential candidate for the boundary of $SM(PO_{lb})$.

It is remarkable that, even though the basin boundary of PO_{ub} and the torus orbit are no longer present, the behavior of the edge remains unvaried. Therefore the edge is not related to the presence of a second basin of attraction besides the laminar one.

5.2.2 $R_{sn} < R < R_c$

Finally, we consider the case with $R_{sn} < R < R_c$. The multipliers of PO_{ub} greater than one become real, which forecasts the disappearance of the spiraling behavior of $SM(PO_{lb})$ and $UM(PO_{ub})$. Indeed, a sample of initial conditions from a point in B_s to a point on PO_{ub} shows no 'peaks' and 'steps' in relaminarization time. The lifetime is gradually increasing starting from the point on B_s and moving toward the point on PO_{ub} (Fig. 11A,B), where it has a maximum. After PO_{ub} the lifetime decreases and sets to a quite constant value, higher than before the point on PO_{ub}. Only a hint of the edge remained: a single step in lifetime crossing PO_{ub}.

How did $UM(PO_{ub})$ change? Because the multipliers are real, $UM(PO_{ub})$ has two distinct directions: $UM_1(PO_{ub})$, associated with the most unstable eigenvector v_1, and $UM_2(PO_{ub})$, associated with the least unstable eigenvector v_2. $UM1(PO_{ub})$ is easily tracked starting a initial condition along on v_1 and $-v_1$: both arcs of $UM1(PO_{ub})$ are connected directly to the origin. $UM2(PO_{ub})$ is more difficult to follow because initial conditions on v_2 are attracted to $UM1(PO_{ub})$. Using a bisection technique, and exploiting the fact that initial conditions on different sides are attracted to different arcs of $UM1(PO_{ub})$, we find an arc of $UM2(PO_{ub})$ which is connected directly to PO_{lb}, without any spiraling structure (Fig. 11C). The bisection technique is not able to find the other arch of $UM2(PO_{ub})$, and we suppose that this arch is connected directly to the origin (Fig. 11D).

In this configuration the edge behavior is present but strongly reduced. Trajectories on the upper side of the edge have to circumnavigate PO_{ub} before reaching the origin, but they are not slowed by the complicated path imposed by the spiral.

6 Discussion

The following dynamical portrait emerges from the study of a six dimensional model for shear turbulence. For $R > R_t$ there is a stable periodic orbit with a finite basin of attraction D. A periodic orbit on a torus is embedded in ∂D. The unstable manifold of the torus orbit, $UM(T)$, has a convoluted structure, which in a two dimensional projection appears

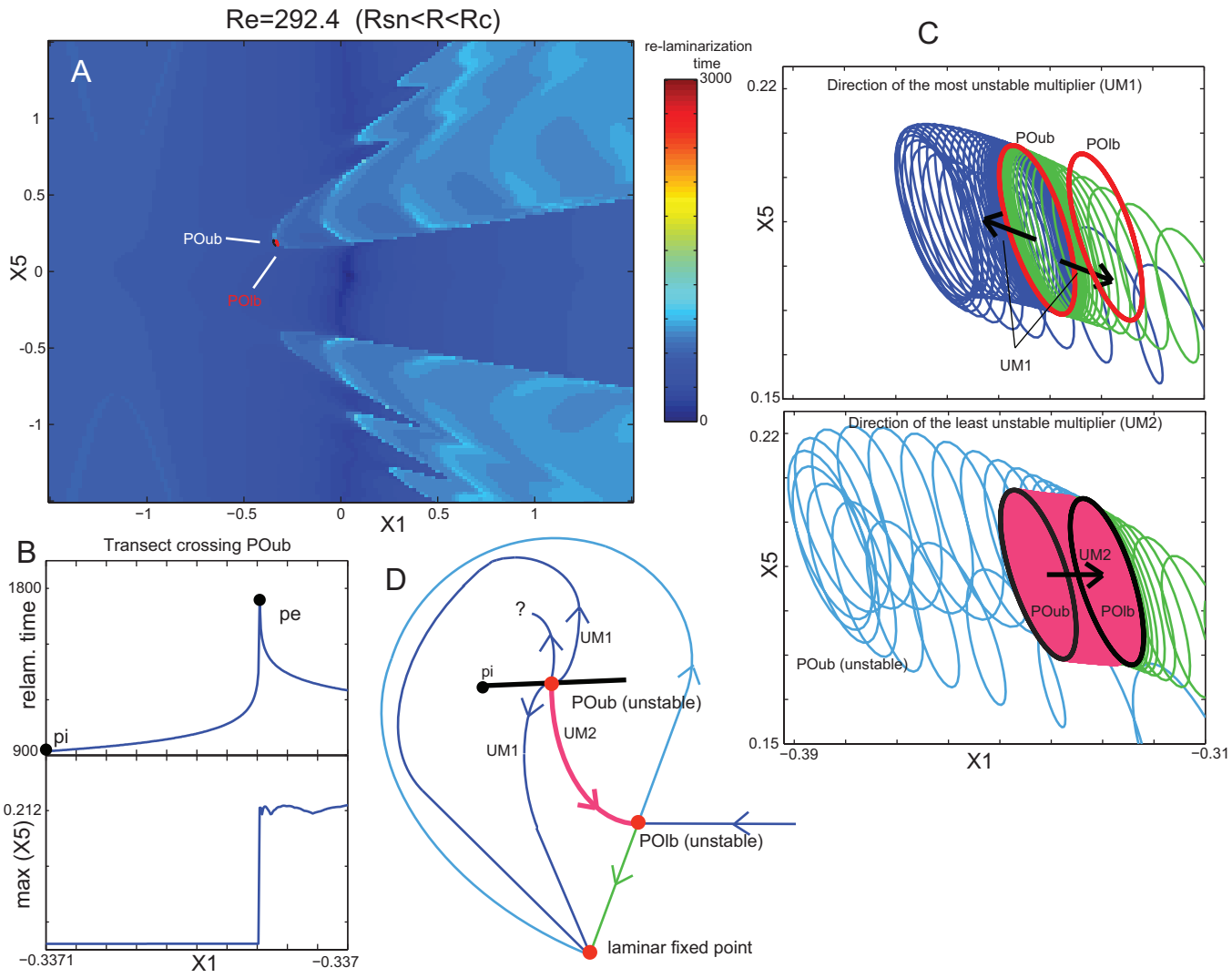

Figure 11: A) Lifetime of trajectories and projection of PO_{ub} and PO_{lb}, as in Figure 5 and Figure 10, but with $R = 292.4$ ($R_{sn} < R < R_c$). B) Analysis of a transect of initial conditions crossing PO_{ub}. The point p_i corresponds to an initial condition that relaminarizes 'directly', while the point p_e corresponds to an initial condition on PO_{ub}. C) Directions of the unstable manifolds of PO_{ub}: UM_1 is associated with the most unstable multiplier, UM_2 is associated with the other unstable multiplier. D) Cartoon of the phase space, with the laminar fixed point, PO_{ub}, PO_{lb}, and unstable manifolds of PO_{ub}.

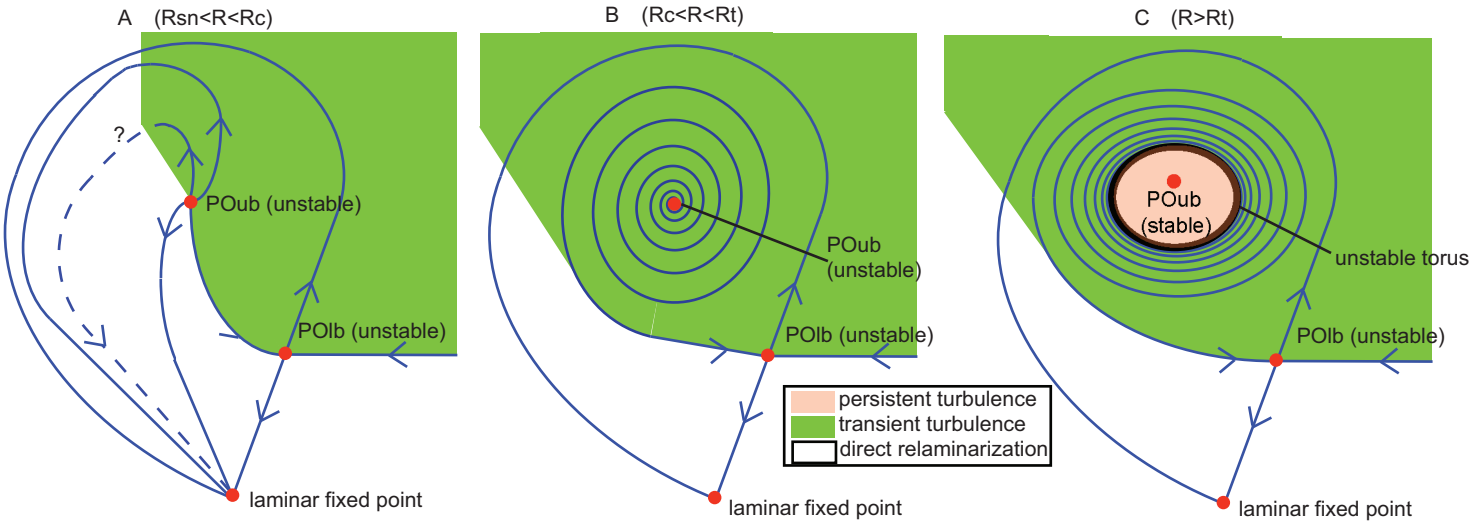

Figure 12: Cartoon of the phase space for different values of R. A) $R_{sn} < R < R_c$, two unstable periodic orbits, both with real unstable multipliers. B) $R_c < R < R_t$, two unstable periodic orbits; the upper one with two complex conjugate unstable multipliers, the lower one with a real unstable multiplier. C) $R > R_t$, stable and unstable periodic orbits. The unstable orbit has a real unstable multiplier. The color shading indicates in an approximate way regions with different relaminarization behavior.

as a spiral. This unstable manifold intersects the stable manifold of an unstable periodic orbit $SM(PO_{lb})$ (Fig. 12C).

$SM(PO_{lb})$ is technically part of the boundary of B, because every neighborhood of $SM(PO_{lb})$ contains at least one point of B (e.g., orbits that relaminarize) and at least one point not of B (e.g., orbits that collapse to PO_{lb}). However, the basin boundary nature of $SM(PO_{lb})$ is not intuitive, since orbits on both sides of $SM(PO_{lb})$ relaminarize. $SM(PO_{lb})$ divides orbits with different qualitative behavior belonging to the same basin of attraction, and hence it is an edge. The different qualitative behavior emerges because orbits on the side of the stable manifold opposite to the origin need to circumnavigate this object in order to relaminarize. The path followed by the orbits is complicated by the coiling structure of $SM(PO_{lb})$ around the basin of attraction of PO_{ub}. Orbits starting between the folds of the unstable manifold have to uncoil before reaching the origin. This is apparent in the two dimensional representation in Figure 7.

We propose the following analogy: the basin of attraction of PO_{ub} represents persistent turbulence, i.e. flows that never decay to laminar. Trajectories between the folds of $SM(PO_{lb})$ represent instead transient turbulence: complex flows which eventually decay to the laminar state. The edge structure divides orbits that relaminarize in a simple fashion from orbits that experience transient turbulence.

For $R_c < R < R_t$ the upper branch periodic orbit becomes unstable. The basin boundary of this orbit disappear, the torus collapses to PO_{ub}, and $UM(PO_{ub})$ takes the place of $UM(T)$. This unstable manifold continues to be a spiral, and continues to intersect $SM(PO_{lb})$ (Fig. 12B). The structure of the edge remains unchanged. To continue the

analogy, the case $R_c < R < R_t$ describes a situation in which no sustained turbulence is possible. All the observed turbulence must be transient.

Finally, for $R_{sn} < R < R_c$ the multipliers of PO_{ub} become real, and the spiraling behavior ceases to exist. One arc of $UM(PO_{ub})$ continues to intersect $SM(PO_{lb})$. Since this stable manifold is no longer a spiral, the edge effect is strongly reduced. The edge is still present as a single fold, which divides trajectories that go straight to the origin from those that have to circumnavigate PO_{ub} (Fig. 12A).

These results show many similarities with the two-dimensional model studied by Lebovitz [5]. The model in [5] shows, for a certain range of a Reynolds-like parameter R^*, an upper and lower fixed point and an unstable periodic orbit, which are the analogues of PO_{ub}, PO_{lb} and the torus orbit of our model. For smalls value of R^* the upper fixed point is stable and the periodic orbit constitutes its basin boundary. The stable manifold of the lower branch point spirals around the periodic orbit and coincides with its unstable manifold. This situation clearly represents a 2D analogue of our model for $R > R_t$. For higher values of R^* the upper fixed point becomes unstable and the periodic orbit disappears. The stable manifold of the lower fixed point is now spiraling around the upper fixed point and coincides with its unstable manifold. This situation is analogous to our model for $R_c < R < R_t$.

Some differences are present between the two models. First, because Lebovitz's model is 2D, the stable and unstable manifolds of the different objects can have the same dimension and hence coincide. Second, the additional basin of attraction is present for small values of R^* and disappears for high R^*, while in our model it appears for high values of R. These differences should warn about the variability of results between simplified models. However, the analogies suggest the presence of common features in shear turbulence models.

The portrait emerging from the model proposed here and the model of Lebovitz give a simple interpretation of the edge. The fact that the edge coincides with a stable manifold of an invariant object was already known [12, 10, 11]. The novelty of our results is that one limb of the edge does not extend to infinity, but connects to another invariant object, which for the case here studied can be a fixed point, a simple periodic orbit or a torus orbit. If this stable manifold is spiraling around the invariant object, then the difference in relaminarization time between trajectories starting on different sides of the edge is enhanced. However, we should stress that the spiral structure is not strictly necessary for the presence of the edge. In higher dimensional models, the full NS as the limit, we expect the invariant objects and the manifolds to be more convoluted than in a two or six dimensional model. As a consequence, we expect a greater difference in trajectories on different side of the edge, with or without the presence of a spiral behavior.

Finally, the edge seems to be related to the unstable manifold of this invariant object, but dimensional considerations imply that these two cannot coincide. We conclude that the stable and unstable manifold intersect, but more investigation are needed to draw more specific conclusions.

7 Conclusion

A six-dimensional system of ODEs representing a Galerkin truncated model for Plane Poiseuille Flow was derived and analyzed. In this model the edge behavior is explained by the combination of simple dynamical elements: the stable manifold of an invariant ob-

ject connected to another invariant object. This configuration is possible with or without the presence of another basin of attraction besides the laminar one, and with or without a spiraling stable manifold.

8 Acknowledgment

I would like to thank the directors of the Geophysical Fluid Dynamics Program for the opportunity of this great experience. I would like to thank all the lecturers and speakers for sharing their knowledge. In particular, I'm deeply grateful to Norman Lebovitz for his support on this project. Finally, I would like to thank all the participants and the fellows for the beautiful time spent together.

References

[1] O. Dauchot and N. Vioujard, *Phase space analysis of a dynamical model for the subcritical transition to turbulence in plane couette flow*, The European Physical Journal B - Condensed Matter and Complex Systems, 14 (2000), pp. 377–381.

[2] A. Dhooge, W. Govaerts, and Y. A. Kuznetsov, *matcont: A matlab package for numerical bifurcation analysis of odes*, ACM TOMS, 29 (2003), pp. 141–164.

[3] J. M. Hamilton, J. Kim, and F. Waleffe, *Regeneration mechanisms of near-wall turbulence structures*, Journal of Fluid Mechanics, 287 (1995), pp. 317–348.

[4] N. Lebovitz, *Shear-flow transition: the basin boundary*, Nonlinearity, 22 (2009), pp. 2645, 2655.

[5] ——, *Boundary collapse in models of shear-flow turbulence*, Communications in Nonlinear Science and Numerical Simulations, doi:10.1016/j.cnsns.2011.07.023q (2010).

[6] J. Moehlis, H. Faisst, and B. Eckhardt, *A low-dimensional model for turbulent shear flows*, New Journal of Physics, 6 (2004), pp. 1–17.

[7] J. Moehlis, H. Faisst, and B. Eckhardt, *Periodic orbits and chaotic sets in a low-dimensional model for shear flows*, J. Applied Dynamicl Systems, 4 (2005), pp. 352–376.

[8] S. A. Orszag, *Accurate solution of the orr-sommerfeld stability equation*, Journal of Fluid Mechanics, 60 (1971), p. 689703.

[9] T. M. Schneider, F. De Lillo, J. Buehrle, B. Eckhardt, T. Dörnemann, K. Dörnemann, and B. Freisleben, *Transient turbulence in plane couette flow*, Phys. Rev. E, 81 (2010), p. 015301.

[10] T. M. Schneider, B. Eckhardt, and J. A. Yorke, *Turbulence transition and the edge of chaos in pipe flow*, Phys. Rev. Lett., 99 (2007), p. 034502.

[11] T. M. Schneider, J. F. Gibson, M. Lagha, F. De Lillo, and B. Eckhardt, *Laminar-turbulent boundary in plane couette flow*, Phys. Rev. E, 78 (2008), p. 037301.

[12] J. D. Skufca, J. A. Yorke, and B. Eckhardt, *Edge of chaos in a parallel shear flow*, Phys. Rev. Lett., 96 (2006), p. 174101.

[13] J. Vollmer, T. M. Schneider, and B. Eckhardt, *Basin boundary, edge of chaos, and edge state in a two-dimensional model*, New Journal of Physics, 11 (2009), p. 013040.

[14] F. Waleffe, *On a self-sustaining process in shear flows*, Physics of Fluid, 9 (1997), pp. 883–900.

[15] ——, *Homotopy of exact coherent structures in plane shear flows*, Physics of Fluids, 15 (2003), pp. 1517–1534.

[16] J. Wang, J. Gibson, and F. Waleffe, *Lower branch coherent states in shear flows: Transition and control*, Phys. Rev. Lett., 98 (2007), p. 204501.